Robust Flutter Margins of an F/A-18 Aircraft from Aeroelastic Flight Data

Rick Lind* and Marty Brenner[†]

NASA Dryden Flight Research Center, Edwards, California 93523-0273

It is essential to determine flight conditions at which aeroelastic instabilities occur. Flight-test methods can be dangerous and costly, whereas analytical methods may not accurately predict the flutter boundary. An approach to computing flutter boundaries based on the structured singular value is presented. The aeroelastic system is formulated in a robust stability framework by parameterizing around dynamic pressure and introducing uncertainty operators to account for modeling errors. Flight data can be used to validate the robust system model and increase accuracy of the flutter margin estimate. Flutter margins are generated for the F/A-18 Systems Research Aircraft using this method and traditional methods. Extensive flight data from conditions throughout the flight envelope are analyzed to determine the levels of uncertainty in a theoretical model. The robust margins demonstrate that the flight conditions for flutter may lie closer to the flight envelope than previously estimated by traditional analysis.

Nomenclature

C	=	damping matrix
K	=	stiffness matrix
M	=	mass matrix
Q	=	unsteady aerodynamic force matrix
$\bar{q}$	=	dynamic pressure
W_{in}	=	weighting for plant input uncertainty
Δ	=	structured uncertainty operator
Δ_A	=	state matrix uncertainty operator
Δ_{in}	=	plant input uncertainty operator
$\delta_{\bar{q}}$	=	perturbation in dynamic pressure
μ	=	structured singular value

I. Introduction

AEROELASTIC flutter is a potentially destructive instability resulting from an interaction between aerodynamic, inertial, and structural forces.[1] Design of a new aircraft, or even a configuration change of a current aircraft, requires study of the aeroelastic stability before a safe flight envelope can be determined. The aeroelastic community has identified several areas of research that are essential for developing an accurate flutter test program.[2] These areas focus on the dramatic time and cost associated with safely expanding the flight envelope to ensure no aeroelastic instabilities are encountered.

An important research topic for aeroelasticity engineers is the development of more confident flutter or instability margins. Flight envelope expansion is a dangerous and costly process due to poor flight-test methods of predicting flutter.[3] These methods usually rely on tracking modal damping trends, estimated from flight data, which are not always accurate indicators of flutter onset. Often the error in the estimates is quite large and trends may show little variation until a drastic and sudden change near flutter.

Several analytical methods were developed to determine the conditions for aeroelastic instability. A traditional method, known as the p–k method,[4] utilizes a structural model coupled with equations for the unsteady aerodynamics. This method is based on a finite element model of the aircraft and does not directly consider flight data from the physical aircraft. Another method is based on a parameter estimation algorithm that utilizes flight data to formulate elements of a state-space model.[5] This method suffers from poor excitation and data measurements that may lead to inaccurate modal parameters.

A novel approach to computing flutter instability boundaries is developed that utilizes a theoretical model while directly accounting for variations with flight data. The aeroelastic stability problem is formulated in a framework suitable for well-developed robust stability theory. Flight data are analyzed to describe a set of uncertainty operators that account for variations between the theoretical model and the physical aircraft. A robust stability measure known as the structured singular value μ (Ref. 6) is used to compute flutter boundaries that are robust to these variations. In this sense, a worst-case flutter boundary is computed that directly accounts for flight data.

This method presents several advantages to traditional flutter boundary estimation methods. The analytical system is able to better represent the aircraft dynamics by coupling the finite element model with actual flight data through the uncertainty operators. The resulting robust margins are guaranteed to be worst case with respect to the indicated amount of modeling uncertainty. This procedure may greatly reduce the time and cost associated with experimental flight envelope testing because the instability limits may be more accurately and confidently identified. Additionally, the uncertainty levels in the theoretical model may be determined using flight data from a safe flight condition without requiring the aircraft to approach a flutter instability point.

Robust, or worst-case, flutter margins for the F/A-18 Systems Research Aircraft (SRA) are computed. The F/A-18 SRA is being flown at NASA Dryden Flight Research Center with a wing tip excitation system shown in Fig. 1. This aircraft is a two-seat configuration fighter with production engines. Recent flutter testing was initiated due to a structural modification to the left wing. Internal fittings and external fairings had to be replaced with larger and heavier items to accommodate advanced aileron concepts to be implemented and flown. The flight data presented in this paper were generated using the new attachments but with a standard aileron.

The flutter results represent a significant improvement to accepted flutter results for the F/A-18 SRA computed using the traditional p–k method. Nominal flutter margins computed using the μ method but ignoring all uncertainty operators are shown to match closely with the p–k method flutter margins. This result lends validity to the μ method as an accurate indicator of flutter instability. Directly accounting for modeling uncertainty and flight data variations in the μ-based flutter analysis generates robust flutter margins that are more conservative than the nominal margins. These robust flutter margins are accepted with more confidence than the nominal margins because they are based on flight-test data rather than a purely theoretical model.

*National Research Council Postdoctoral Research Fellow, MS 4840D/RC. E-mail: lind@xrd.dfrc.nasa.gov. Member AIAA.

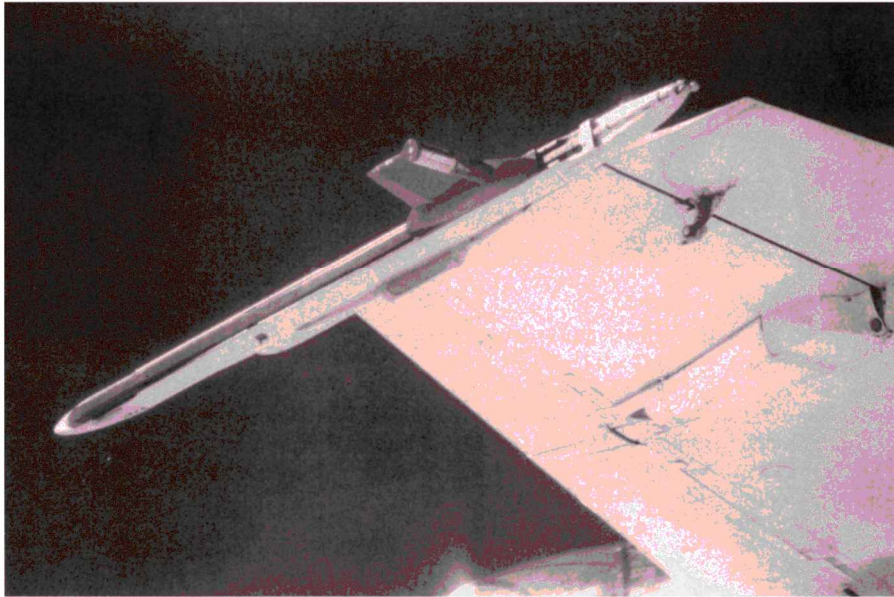†Research Engineer, MS 4840D/RC. E-mail: gonzo@xrd.dfrc.nasa.gov.

Fig. 1   F/A-18 wing with wing tip exciter.

II.   Robust Stability and μ

Any aeroelastic model is an approximate representation of the aircraft dynamics. Inaccuracies in the model, such as errors in coefficients and unmodeled dynamics, must be considered in the stability analysis and control synthesis procedures. Uncertainty operators are included in the system model to account for these inaccuracies in the robust stability framework.

The uncertainty operator Δ is allowed to lie within a norm bounded set. This leads to the consideration of a family of plant models. Weighting matrices are usually included in the μ framework to normalize the uncertainty norm bound to unity

$$\Delta = \{\Delta : \|\Delta\|_\infty \le 1\}$$

The structured singular value μ can be used to determine robustness of the plant to structured modeling uncertainty. The μ framework allows for a rich class of uncertainty descriptions to accurately account for variations with the true physical system. Two types of blocks, repeated scalar and full block matrices, are used to define uncertainty operators. Real parametric uncertainty is allowed to enter the problem as a scalar or repeated scalar element, whereas complex uncertainty may enter as scalar, repeated scalar, or full block.

Define the structured singular value μ,

$$\mu(P) = \frac{1}{\min\{\bar{\sigma}(\Delta) : \Delta \in \Delta, \det(I - P\Delta) = 0\}}$$

with $\mu(P) = 0$ if no Δ exists such that $\det(I - P\Delta) = 0$. Singular value μ is an exact measure of robustness for systems with structured uncertainty. The inverse of μ can be interpreted as a measure of the smallest destabilizing perturbation. The system is guaranteed to be robustly stable for all uncertainty operators bounded by the smallest destabilizing value.

Unfortunately, μ is difficult to compute. Upper and lower bounds for μ have been derived, which utilize two sets of structured scaling matrices.[7] These scaling matrices are similar in structure to the uncertainty block structure and commute with the uncertainty elements. An upper bound can be written as a linear matrix inequality by considering a maximum eigenvalue condition utilizing the structured scaling matrices.[6]

III.   Robust Flutter Margin Formulation

A.   Linear Aeroelastic Model

Consider the generalized equation of motion for the aeroelastic response of the aircraft[8]:

$$M\ddot{\eta} + C\dot{\eta} + K\eta + \bar{q}Q(s)\eta = 0$$

For a system with n modes, define $M \in R^{n \times n}$ as the mass matrix, $C \in R^{n \times n}$ as the damping matrix, and $K \in R^{n \times n}$ as the stiffness matrix. Here, $\bar{q} \in R$ is a scalar representing the dynamic pressure, and $Q \in C^{n \times n}$ is the frequency varying matrix of unsteady aerodynamic forces.

Values of the aerodynamic force matrix at distinct frequencies can be derived using finite element models of the aircraft and panel methods for unsteady force calculations. A computer program developed for NASA known as STARS[9] is utilized. This code solves the subsonic aerodynamic equations using the doublet lattice method.[10] The supersonic forces are generated using a different approach known as the constant panel method.[11]

The unsteady aerodynamic forces are fit to a standard finite-dimensional state-space system. At low frequencies near the flutter modes, this form encompasses the traditional Padé approximation and low-order Roger[12] formulations, which use lag terms for the transient aerodynamics,

$$Q(s) = \left[\begin{array}{c|c} A_Q & B_Q \\ \hline C_Q & D_Q \end{array}\right] = D_Q + C_Q(sI - A_Q)^{-1}B_Q$$

Given the number of structural modes, n, and the number of aerodynamic states, n_Q, define $A_Q \in R^{n_Q \times n_Q}$, $B_Q \in R^{n_Q \times n}$, $C_Q \in R^{n \times n_Q}$, and $D_Q \in R^{n \times n}$ as the state-space elements of $Q(s)$.

A state-space system is formulated utilizing the generalized states, η and $\dot{\eta}$, and the unsteady aerodynamic states x. The state update matrix is determined by the following three linear equations:

$$\begin{bmatrix} \dot{\eta} \\ \ddot{\eta} \\ \dot{x} \end{bmatrix} = \begin{bmatrix} 0 & I & 0 \\ -M^{-1}(K + \bar{q}D_Q) & -M^{-1}C & -\bar{q}M^{-1}C_Q \\ B_Q & 0 & A_Q \end{bmatrix} \begin{bmatrix} \eta \\ \dot{\eta} \\ x \end{bmatrix}$$

B.   Parameterization over Flight Condition

The μ-analysis method considers stability over a range of flight conditions to determine the onset of flutter. This is accomplished by parameterizing the state-space system model around dynamic pressure. The generalized equation of motion is a linear function of $\bar{q}$ so that perturbations to this parameter can enter as a linear fractional transformation.[6] The μ will treat the perturbation as a system uncertainty, and the resulting stability margin will indicate what changes in dynamic pressure will cause the onset of flutter.

Consider an additive perturbation, $\delta_{\bar{q}} \in R$, on the nominal dynamic pressure $\bar{q}_{\text{nom}}$,

$$\bar{q} = \bar{q}_{\text{nom}} + \delta_{\bar{q}}$$

Replace $\bar{q}$ with the perturbed form in the generalized equation of motion and separate terms involving the perturbation $\delta_{\bar{q}}$. Introduce

this perturbation as an external operator affecting the nominal system. Additional input and output signals, w and z, are associated with the nominal system to relate the perturbation operator,

$$w = \delta_{\bar{q}} z$$

The nominal state-space aeroelastic model is formulated with the additional signals to account for the parameterization of the dynamic pressure. Define the plant $P(s)$ such that $z = P(s)w$, where z and w are determined by the following equations:

$$
\begin{bmatrix} \dot{\eta} \\ \ddot{\eta} \\ \dot{x} \\ \hline z \end{bmatrix} =
\left[\begin{array}{ccc|c}
0 & I & 0 & 0 \\
-M^{-1}(K + \bar{q}_{\text{nom}}D_Q) & -M^{-1}C & -\bar{q}_{\text{nom}}M^{-1}C_Q & -I \\
B_Q & 0 & A_Q & 0 \\
\hline
M^{-1}D_Q & 0 & M^{-1}C_Q & 0
\end{array}\right]
\begin{bmatrix} \eta \\ \dot{\eta} \\ x \\ \hline w \end{bmatrix}
$$

It is straightforward to demonstrate the robust formulation of the system with the dynamic pressure parameterization equivalent to the nominal state-space system given in the preceding section. Simply compute the closed-loop transfer function with the perturbation $\delta_{\bar{q}} = 0$, and the nominal system is recovered.

C. Uncertainty Operators

Uncertainty operators are included with the linear system to model variations between the theoretical system and the physical aircraft. They also allow the analysis to consider a range of aircraft dynamics that may change due to variations in parameters such as mass or variations in the aerodynamics caused by small deflections in the aircraft surfaces.

Frequency varying weightings are included with each type of uncertainty to normalize the variation such that the uncertainty parameter is norm bounded by one at every frequency. A large weighting over a frequency range indicates large errors are possible between the analytical model and the physical system throughout those frequencies.

Experimental flight data can be used to generate these weightings. Transfer functions of the analytical model can be compared with experimental flight data transfer functions. Different size perturbations are allowed to affect specific system parameters to the degree that the resulting transfer functions cover the range of experimental flight data.

Model validation algorithms are used to verify that the amount of uncertainty in the linear model is sufficient to generate the flight data sets. An algorithm based on μ-analysis of the linear system with frequency domain flight data[13] is used. The model validation condition is derived as a standard μ calculation. The μ value at each frequency relates the required size of perturbations at that frequency. This information is used to compute frequency varying weightings to scale the uncertainty set. The model validation procedure is repeated until a small amount of uncertainty is defined that still validates the model but reduces the conservatism in the resulting flutter analysis.

IV. Robust Flutter Margin

Flutter margins are computed using μ-analysis on the parameterized linear system with associated uncertainty operators. The flutter margin is the smallest destabilizing perturbation to dynamic pressure for the linear system with the given amount of modeling uncertainty. The μ value directly accounts for the associated operators to compute a worst-case margin with respect to the entire range of uncertainty.

Nominal flutter margins are computed for the aeroelastic system with dynamic pressure parameterization but no modeling uncertainty operators. The nominal margins should be similar to traditional p–k margins because each method utilizes the finite element model and unsteady aerodynamic forces with no associated uncertainty operators.

Robust flutter margins are determined by computing μ with respect to the modeling uncertainty. The margin is the largest perturbation to dynamic pressure for which the system remains stable in the presence of the norm bounded uncertainty operators. Including the uncertainty in the analysis will increase the conservatism of the flutter margin due to the worst-case nature of the μ computation.

Value μ is a much more informative stability margin and presents several advantages as compared to flight flutter test parameters such as pole location and damping. The conservatism introduced by considering the worst-case uncertainty perturbation is a measure of sensitivity. Robust μ values, which are significantly different than the nominal values, indicate the aircraft is highly sensitive to modeling errors and changes in flight condition. The μ lower bound computes a worst-case uncertainty operator within the norm bounded set, which provides information about the worst-case system dynamics and associated flutter mechanism and may extend to indicate active and passive control strategies for flutter suppression.

Additionally, damping is only truly informative at the point of instability because stable damping and damping trends at a given flight condition do not guarantee what increases in dynamic pressure may be safely considered. Value μ computes the smallest destabilizing perturbation, which indicates the nearest flight conditions that will cause a flutter instability. In this respect, μ is a stability predictor whereas damping is merely a stability indicator.

These characteristics of μ make the worst-case flutter algorithm especially valuable for flight-test programs. Aeroelastic flight data can be measured at a stable flight condition and used to evaluate uncertainty operators. The μ method, unlike damping estimation, does not require the aircraft to approach instability for accurate prediction. Value μ can be computed to update the stability margins with respect to the new uncertainty levels. The worst-case stability margin then indicates what flight conditions may be safely considered for safe and efficient expansion of the flight envelope.

V. Aeroelastic Flight Data

A. Excitation System

Extensive flight data from the F/A-18 SRA are used to generate uncertainty descriptions for an analytical aircraft model.[14] Over 30 flights were conducted in two sessions between September 1994 and February 1995 and between June 1995 and July 1995 at NASA Dryden Flight Research Center. Each flight performed maneuvers for different conditions throughout the flight envelope. A total of 260 different data sets are generated from various conditions throughout the flight envelope.[15]

The aeroelastic flight data are generated using an external structural excitation system developed by Dynamic Engineering Incorporated (DEI). This DEI exciter is a modification of an excitation system used for F-16 XL flutter research.[16,17] The system consists of a wing tip exciter, an avionics box mounted in the instrumentation bay, and a cockpit controller.

Aerodynamic forces are generated by the wing tip exciter. This exciter consists of a small fixed aerodynamic vane forward of a rotating slotted hollow cylinder. Rotating the cylinder varies the pressure distribution on the vane and results in a wing tip force changing at twice the cylinder rotation frequency. The magnitude of the resulting force is determined by the amount of opening in the slot. The F/A-18 aircraft with a left-side wing tip exciter is shown in Fig. 1.

The cockpit controller commands a frequency range, duration, and magnitude for the wing tip excitation signal. Frequency varying excitation is generated by changing the cylinder rotation frequency with sine sweeps. Each wing tip exciter is allowed to act in-phase, 0 deg, or out-of-phase, 180 deg, with each other. Ideally, the in-phase data excite the symmetric modes of the aircraft and the out-of-phase data excite the antisymmetric modes.

Flight data sets are recorded by activating the exciter system at a given flight condition. The aircraft attempts to remain at the flight condition throughout the series of sine sweeps desired by the controller. The sine sweeps were restricted to within 3 and 35 Hz. Smaller ranges were sometimes used to concentrate on a specific set of modal responses. Multiple sets of either linear or logarithmic sweeps were used with the sweep frequency increasing or decreasing.
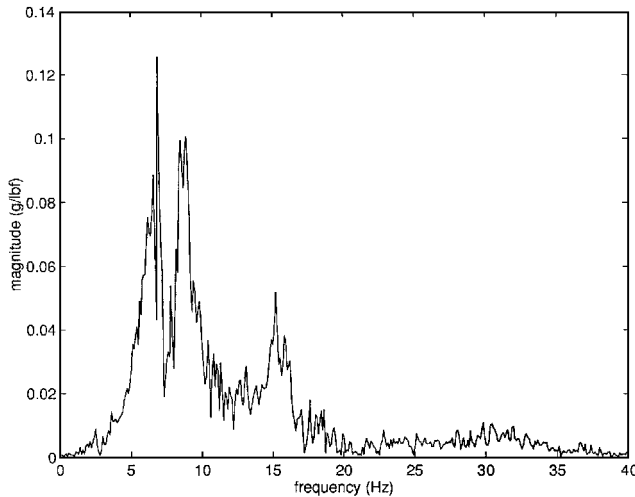
Fig. 2 Flight data transfer function from symmetric excitation to left wing leading-edge accelerometer at Mach = 0.8 and 30,000 ft.

B. Data Analysis

Aeroelastic flight data generated with the DEI exciter system are analyzed by generating transfer functions from the excitation force to the sensor measurements. Figure 2 presents a flight data transfer function generated with Fourier analysis. There are several inherent assumptions associated with Fourier analysis that are violated with the flight data. The assumptions of time-invariant stationary data composed of sums of infinite sinusoids are not met by these transient response data. The analysis presented is based on Fourier analysis, although current research investigates wavelet techniques to analyze the flight data.[15]

The excitation force is not directly measured but rather a strain gauge measurement is used to estimate this force. The strain gauge records a point response at the exciter vane root, which is considered representative of the distributed excitation force load over the entire wing surface. Vane root strain is assumed to be directly proportional to the vane airloads due to excitation.

There are several undesired behaviors demonstrated by these exciters in flight.[15] The exciters displayed erratic behavior at higher dynamic pressures due to binding in both the motor drive mechanism and rotating cylinders. At low dynamic pressures the system operated better but still displays some phase drift between the left and right cylinder rotations. Additionally, excitation sine sweeps of increasing frequency generally excited different modes than sweeps of decreasing frequency despite identical flight conditions.

The effect of the poor approximation to input force and the erratic behavior of the exciters is to reduce the quality of the flight data. Methods relying on system identification fail to accurately utilize the data to predict a flutter boundary.[18] The μ method is able to account for the data anomalies by including greater levels of uncertainty.

VI. Aircraft Model

A. Nominal Theoretical Models

The generalized equations of motion are used to derive a linear, finite-dimensional state-space model of the aircraft. This model contains 14 symmetric structural modes, 14 antisymmetric structural modes, and 6 rigid-body dynamic modes. The control surfaces are not active, and no control modes are included in the model.

A finite element model of the SRA is used to compute the modal characteristics of the aircraft. Frequencies of the dominant modes for flutter are presented in Table 1. These modal frequencies are computed for the aircraft with no aerodynamics considered. The predicted flutter results for this aircraft are computed from the finite element model using the p–k method. A detailed explanation of the SRA flutter analysis using traditional methods is given in Ref. 19.

The doublet lattice and constant panel methods are used to compute the frequency varying unsteady aerodynamic forces for several subsonic, transonic, and supersonic Mach numbers. Force matrices for Mach numbers $M = 0.8, 0.9, 0.95, 1.1, 1.2, 1.4,$ and 1.6 are available. The unsteady aerodynamic forces are computed as a

Table 1 Modal frequencies

Mode	Symmetric, Hz	Antisymmetric, Hz
Wing first bending	5.59	8.84
Fuselage first bending	9.30	8.15
Wing first torsion	13.98	14.85
Wing second bending	16.95	16.79
Wing outboard torsion	17.22	——
Fuselage second bending	19.81	18.62
Fuselage torsion	——	24.19
Wing second torsion	29.88	29.93

function of reduced frequency k,

$$k = \omega(\bar{c}/2V)$$

The reduced frequency is a function of the true frequency ω, the true velocity V, and the mean aerodynamic chord $\bar{c}$. Aerodynamic forces generated for 10 reduced frequency points between $k = 0.0001$ and $k = 4$ are sufficient for flutter margin computation for this aircraft.

The unsteady aerodynamic forces are fit to a finite-dimensional state-space system. The system identification algorithm is a frequency domain curve fitting algorithm based on a least squares minimization. A separate system is identified for each column of the unsteady forces transfer function matrix. Fourth-order state-space systems are used for each column of the symmetric forces and second-order state-space systems are used for each column of the antisymmetric forces. These systems are combined to form a single multiple-input and multiple-output state-space model of the unsteady aerodynamics forces, previously designated $Q(s)$, with 56 states for the symmetric modes and 28 states for the antisymmetric modes.

The analytical aeroelastic model has inputs for symmetric and antisymmetric excitation forces. It is assumed the excitation force will be purely symmetric or antisymmetric. There are six sensor measurements generated by accelerometers at the fore and aft of each wing tip and on each aileron.

B. Uncertainty Descriptions

Noise and uncertainty operators are introduced to the linear aeroelastic model to account for variations between the analytical model and the actual aircraft. Standard analysis of the linear model is used to determine the framework for how uncertainty operators enter the system. Two uncertainty operators and a single noise input are used to describe the modeling uncertainty in the linear aeroelastic model. The magnitude of each uncertainty operator and the noise level is determined both from reasoning of the modeling process and analysis of the flight data.[14]

An uncertainty operator Δ_A is associated with the state matrix of the F/A-18 linear model. This uncertainty models variations in both the natural frequency and damping values for each mode. State matrix uncertainty can account for errors in coefficients of the equations of motion and changes in the aircraft dynamics due to parameter variations such as mass consumption during flight.

Δ_A is a structured diagonal matrix with real scalar parameters as elements. Separate elements are used to affect each modal response and time lag in the state matrix. The modal response uncertainty parameters are each repeated two times, whereas each time lag uncertainty appears once on the diagonal.

Each repeated modal uncertainty parameter affects natural frequency and damping by allowing variation in the state matrix elements. Consider formulating the state matrix as block diagonal with a 2×2 block representing each mode. The real component of a modal eigenvalue e_r is the diagonal component of each block whereas the imaginary part e_i is arranged on the off-diagonal positions. Define A_i as the block determining the natural frequency ω_i and damping ζ_i of the ith mode,

$$A_i = \begin{bmatrix} e_r & e_i \\ -e_i & e_r \end{bmatrix} \iff \begin{array}{l} \omega_i = \sqrt{e_r^2 + e_i^2} \\ \zeta_i = -e_r/\omega_i \end{array}$$

Scalar weightings, w_r and w_i, are used to affect the amount of uncertainty in each matrix element. The amount of variation in the

matrix elements and correspondingly the amount of variation in the natural frequency and damping are determined by the magnitude of these scalar weightings. Define $\overline{e_r}$ and $\overline{e_i}$ as elements of the state matrix affected by an uncertainty parameter δ,

$$\overline{e_r} = e_r(1 \pm w_r \delta) \qquad \overline{e_i} = e_i(1 \pm w_i \delta)$$

Aeroelastic modes typically show low damping values caused by the real component being quite small as compared to the imaginary component. Because linear modeling techniques often identify the natural frequency better than the damping value, the weighting for the real component is expected to be larger than that for the imaginary component. This is reflected by the observed modal parameters in the flight data. The natural frequencies show variations of $\pm 5\%$ from the theoretical model whereas the uncertainty in the damping needs approximately $\pm 15\%$ to validate all of the flight data. The scalar weightings are chosen accordingly:

$$w_r = 0.15 \qquad w_i = 0.05$$

The flight data are only able to determine uncertainty levels for the modal parameters of the experimentally observed modes. It is assumed the uncertainty levels in the unobserved modes should be consistent with these values. Parametric uncertainty is introduced for each modal block in the state matrix, affecting observed and unobserved modes, with the weighting values already given.

The single scalar blocks of Δ_A are normalized to 1 by weighting their effect on the time lags of the state matrix. Variations observed in the flight data are used to determine that a weighting of $w_{lag} = 0.15$ is required to admit 15% variation in the time lags.

The second uncertainty operator, Δ_{in}, is a multiplicative uncertainty on the force input to the linear model. This uncertainty is used to cover nonlinearities and unmodeled dynamics. The linear model contains no dynamics above 40 Hz and so the high-frequency component of this operator will reflect this uncertainty. This operator is also used to model the excitation uncertainty due to the DEI exciter system. Analysis of the flight data indicates the input excitation signals rarely had the desired magnitude and phase characteristics that they were designed to achieve. The low-frequency component of the input uncertainty reflects the uncertainty associated with the excitation system used to generate the flight data. The frequency varying transfer function for weighting the input uncertainty is given as

$$W_{in} = 5\frac{s + 100}{s + 5000}$$

A noise signal is included with the sensor measurements. Knowledge of the aircraft sensors is used to determine that a level of 10% noise is possible in the measured flight data. An additional noise may be included on the force input due to the excitation system, but it is decided that the input multiplicative uncertainty is sufficient to describe this noise.

The block diagram for the aeroelastic model with the uncertainty operators is given in Fig. 3. These uncertainty descriptions and levels are used to cover the variations between the analytical model and the flight data over the entire flight envelope.

The flight data used to validate this uncertainty structure cover a large range of flight points. The entire set of 260 flight maneuvers throughout the flight envelope is considered: Mach $\in [0.6, 1.6]$ and altitude $\in [10,000, 40,000]$.
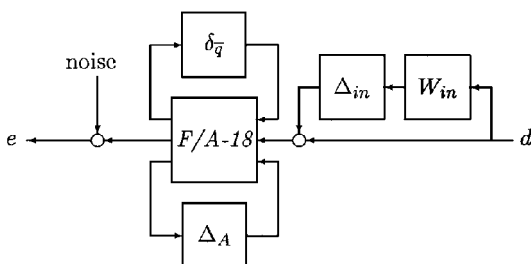

Fig. 3   F/A-18 robust stability block diagram.

Using a single uncertainty description over the entire flight envelope may be conservative. It is reasonable to assume the linear models are more accurate at subsonic and supersonic than at transonic. Additionally, the flight data from the DEI exciter system should be better at subsonic speeds than at supersonic. However, it simplifies the analysis process to consider a single set of uncertainty operators. This process is equivalent to formulating the worst-case uncertainty levels at the worst-case flight condition and assuming that amount of uncertainty is possible for the remaining flight conditions.

VII.   F/A-18 Flutter Points
A.   Nominal and Robust Flutter Margins

Flutter margins are computed for a linear model with the associated modeling uncertainty structure using the μ-analysis method.[20] Linear systems for symmetric and antisymmetric structural modes are separated for ease of analysis. These systems can easily be combined and analyzed as a single system; however, eigenvector analysis would be required to distinguish which critical flutter modes are symmetric and which are antisymmetric. Each system contains the same number of structural modes, 14, and the uncertainty descriptions are identical for each linear model.

The system given in Fig. 3 contains three uncertainty blocks. The parametric uncertainty covering variations due to dynamic pressure $\delta_{\bar{q}}$ is a scalar parameter repeated 14 times, once for each elastic mode. The parametric uncertainty block affecting the modal parameters, Δ_A, is a diagonal matrix with dimension equal to the number of states. Separate scalars along the diagonal represent uncertainty in each elastic mode, each mode in the aerodynamic force approximation, and each lag term. The uncertainty parameters for the modes are repeated two times whereas the parameters for the lag terms are single scalars. Define δ_i as the ith uncertainty parameter for the system with n_m modes and n_l lag terms. The input multiplicative uncertainty block Δ_{in} is a scalar for this single input plant model because we are analyzing symmetric excitation separately from antisymmetric excitation. The uncertainty block structure is

$$\Delta = \mathrm{diag}\left\{ \delta_{\bar{q}} I_{14}, \delta_1 I_2, \ldots, \delta_{n_m} I_2, \delta_{n_m + 1}, \ldots, \delta_{n_m + n_l}, \Delta_{in} \right\}$$

The parametric uncertainty parameters represent changes in elements of the state-space model. The variation of $\delta_{\bar{q}}$ between ± 1 admits dynamic pressures between $0 \le \bar{q} \le 2\bar{q}_{nom}$. Allowing the modal uncertainty parameters, $\delta_1, \ldots, \delta_{n_m}$ to vary between ± 1 allows 5% variation in the imaginary part of the eigenvalue and 15% in the real part. This corresponds to approximately 5% variation in the natural frequency and 15% in the damping value of each mode. These parameters are real quantities. The multiplicative input uncertainty contains magnitude and phase information and is treated as a complex linear time-invariant uncertainty.

Analytical models of the system at different Mach numbers and different altitudes are used to compute flutter boundaries. Numerical differences in the unsteady aerodynamic forces cause the computed flutter margins to be slightly different for plant models with equivalent Mach number but different altitude. The flutter margin is chosen as the worst-case value at the different altitudes analyzed.

Nominal flutter boundaries are initially computed by ignoring the modal and input uncertainties. The μ value is computed only with respect to the parametric uncertainty allowing a range of dynamic pressures to be considered. Robust flutter boundaries are computed with respect to the structured uncertainty set, Δ, described earlier using the structured singular value. Traditional flutter boundaries computed using the p–k method are presented with the nominal and robust flutter boundaries computed with μ in Table 2.

The nominal flutter dynamic pressures computed using the μ method can be directly compared with those computed using the traditional p–k method.[19] Each of these flutter solutions are based on an analytical model with no consideration of modeling uncertainty.

The nominal flutter points for the symmetric modes match closely with the p–k method throughout the flight envelope. The subsonic and supersonic cases show an especially good correlation with the p–k flutter points. For each of these flight regions, the μ-analysis flutter dynamic pressures are nearly identical, within 1%, to the p–k method flutter dynamic pressures. The transonic case at $M = 1.1$, however, shows a slight difference between the two methods. The

Table 2 Nominal and robust flutter points, critical

Mach	Symmetric			Antisymmetric		
	$\bar{q}_{p-k}$	$\bar{q}_{\text{nominal}}$	$\bar{q}_{\text{robust}}$	$\bar{q}_{p-k}$	$\bar{q}_{\text{nominal}}$	$\bar{q}_{\text{robust}}$
0.8	3360	3168	2909	4600	4593	3648
0.9	2700	2706	2575	3150	3057	2944
0.95	2430	2388	2329	2600	2751	2572
1.1	5400	5676	4120	5500	3265	2827
1.2	2469	2454	2327	2850	2893	2653
1.4	3528	3432	3034	4600	4439	4191
1.6	4470	4487	3996	5700	5870	4536

Table 3 Nominal and robust flutter frequencies, critical

Mach	Symmetric			Antisymmetric		
	ω_{p-k}	ω_{nominal}	ω_{robust}	ω_{p-k}	ω_{nominal}	ω_{robust}
0.8	8.2	7.6	7.7	9.0	9.1	9.1
0.9	7.4	7.3	7.3	9.2	9.1	9.2
0.95	6.8	6.9	6.9	9.1	9.2	9.2
1.1	12.1	13.2	13.0	28.6	28.0	28.3
1.2	26.5	27.4	27.4	26.9	28.9	28.9
1.4	28.1	28.1	28.1	30.4	31.7	31.8
1.6	28.9	30.1	30.1	32.8	32.3	32.1

flutter points computed for the μ and $p-k$ methods are 5% apart, which is the largest deviation for the symmetric flutter margins for the Mach numbers considered.

The antisymmetric modes show a similar relationship between the flutter margins computed with the μ and $p-k$ methods. The subsonic and supersonic flutter points are within 5% for the two methods, but there is a greater deviation at the transonic condition. The μ method computes a flutter margin at $M = 1.1$ that is 40% lower than the $p-k$ method indicates.

The nominal flutter points for the μ and $p-k$ methods show the greatest difference for both the symmetric and antisymmetric modes at the $M = 1.1$ transonic case. The aerodynamics at transonic speeds are more difficult to model accurately than at either subsonic or supersonic. Numerical sensitivity makes it difficult to accurately predict the unsteady aerodynamic forces using the panel methods. Similarly, the linearized approximation to the aeroelastic model at transonic is suspect. The μ method makes direct use of the unsteady aerodynamic forces and the corresponding linear model and is affected by the transonic sensitivities.

The robust flutter margins computed using the μ method outlined have lower dynamic pressures than the nominal margin, which indicates the expected conservative nature of the robust computation. These new flutter points are worst-case values for the entire range of allowed uncertainty. The subsonic and supersonic flutter boundaries are not greatly affected by the uncertainty set. In each of these cases, the robust flutter point is within 10% of the nominal flutter point.

The flutter boundary at the transonic case, $M = 1.1$, demonstrates significant sensitivity to the modeling uncertainty. The robust flutter dynamic pressures are approximately 70% of the nominal flutter margins. This is explained by considering the rapid transition of critical flutter boundaries near this region. The critical flutter frequencies and the flutter dynamic pressure widely vary between Mach numbers slightly lower and higher than transonic. The small amount of modeling uncertainty is enough to cause the worst-case flutter mechanism to shift, and the plant assumes characteristics more consistent with a nontransonic regime.

The modal natural frequencies for the critical flutter modes are presented in Table 3. The frequencies computed using the $p-k$ method and the μ-analysis method are close throughout the flight envelope for both the symmetric and antisymmetric modes. Frequencies for the robust flutter solutions are slightly different from the nominal flutter frequencies due to the modeling uncertainty that allowed 5% variation in the modal natural frequencies.

Subcritical flutter margins are computed at dynamic pressures greater than those in Table 2, which indicate flutter instabilities in additional modes. Only nominal subcritical flutter margins are detected with the μ method because the robust flutter margins are

Table 4 Nominal and robust flutter points, subcritical

Mach	Symmetric		Antisymmetric	
	$\bar{q}_{p-k}$	$\bar{q}_{\text{nominal}}$	$\bar{q}_{p-k}$	$\bar{q}_{\text{nominal}}$
0.9			4700	4583
			5300	5093
0.95	7450	6919		
1.1			6050	6001
1.2	5400	5003	8400	7943
1.4	8970	8959		
1.6	8400	8843		
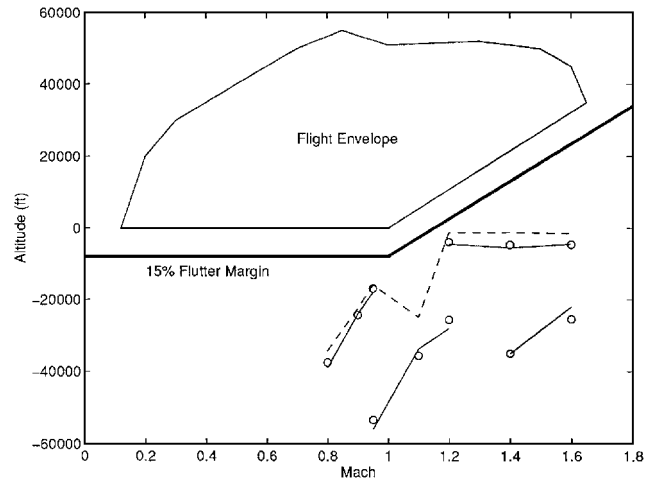
Fig. 4 Nominal and robust flutter points for symmetric modes: ——, nominal $p-k$ margin; ○, nominal μ margin; and - - -, robust μ margin.
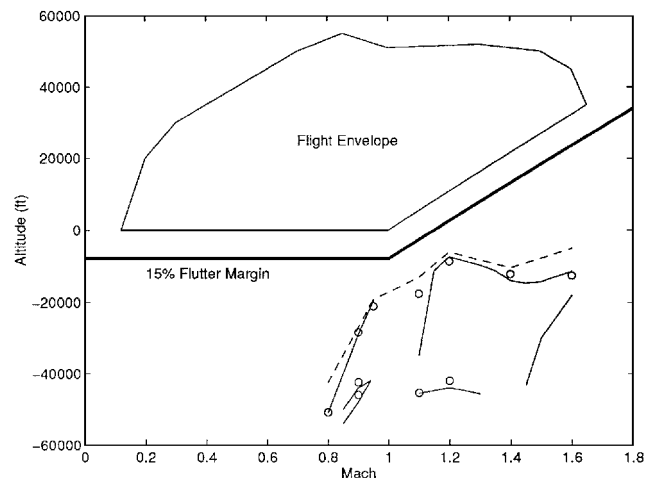
Fig. 5 Nominal and robust flutter points for antisymmetric modes: ——, nominal $p-k$ margin; ○, nominal μ margin; and - - -, robust μ margin.

always worst-case critical margins. The subcritical flutter margins are presented for both the μ and $p-k$ methods in Table 4.

The subcritical flutter margins computed using μ analysis are within 10% of the $p-k$ method subcritical flutter margins for both the symmetric and antisymmetric modes. The μ method is even able to detect the subcritical flutter hump mode occurring for antisymmetric excitation at the 0.9 Mach number.

B. Matched-Point Flutter Margins

The dynamic pressures at which flutter occurs are converted into altitudes, commonly known as matched-point solutions, using standard atmospheric equations. These altitudes are plotted for the symmetric modes in Fig. 4 and for the antisymmetric modes in Fig. 5. The flight envelope of the F/A-18 is shown in these plots along with the required 15% flutter boundary for military aircraft.

Figures 4 and 5 use several short solid lines to indicate the $p-k$ flutter solutions throughout the flight regime. Each of these short

solid lines represents the flutter points due to a specific mode. Flutter points for the symmetric modes given in Fig. 4 show four solid lines indicating three different critical flutter modes for the considered range of Mach numbers along with a subcritical flutter mode occuring at supersonic Mach numbers. The antisymmetric modes show the onset of flutter from two different critical modes along with three subcritical flutter modes throughout the flight envelope in Fig. 5. The frequencies of the critical flutter modes can be found in Table 3.

The subsonic flutter altitudes for both the symmetric modes and the antisymmetric modes demonstrate a similar characteristic. The nominal flutter boundary shows a significant variation from Mach number $M = 0.8$ to 0.95 caused by sensitivity to Mach number for the aeroelastic dynamics associated with the critical flutter modes. The robust flutter boundary indicates the sensitivity of the plant to errors and the worst-case perturbation. The higher altitude for the nominal flutter boundary at Mach number $M = 0.81$ than for Mach number $M = 0.80$ is reflected in the large conservatism associated with the robust flutter boundary. Similarly, slight variation of Mach number near $M = 0.95$ is not expected to increase the nominal flutter boundary so that there is less conservatism associated with the robust flutter boundary.

An interesting trend is noticeable for the symmetric mode robust flutter points in Fig. 4 at the supersonic Mach numbers. The flutter mechanism results from the same modes from $M = 1.2$ to 1.6 with some increase in frequency. Similarly, the altitudes of the nominal flutter margins show little change for these Mach numbers. The aeroelastic dynamics associated with the critical flutter mode are relatively unaffected by the variation of Mach over this range and, consequently, each flutter boundary has the same sensitivity to modeling errors.

The robust flutter margins for the antisymmetric modes at supersonic Mach numbers show a slightly different behavior than the symmetric mode flutter margins. The flutter mechanism is again caused by a single mode from $M = 1.2$ to 1.6 with similar frequency variation as symmetric. The robust flutter margins demonstrate a similar sensitivity to modeling errors at $M = 1.2$ and 1.4 but at $M = 1.6$ a greater sensitivity is shown. The greater conservatism at $M = 1.6$ may indicate impending transition in flutter mechanism from the subcritical mode at slightly higher Mach number.

The altitudes for each nominal and robust flutter condition are below sea level with the subsonic flutter conditions occuring at altitudes significantly below sea level. These negative altitudes correspond to the dynamic pressure values listed in Table 2 in a standard atmosphere. The flutter conditions expressed as dynamic pressures or altitudes convey the same information; however, the matched-point altitude plots more clearly show the flutter conditions for this aircraft are not realistic flight points.

The bold solid line in Figs. 4 and 5 represents the required boundary for flutter points. All nominal and robust flutter points lie outside this region indicating the flight envelope should be safe from aeroelastic flutter instabilities. The robust flutter boundaries computed with μ indicate there is more danger of encountering flutter than was previously estimated with the $p-k$ method. In particular, the robust flutter margin for symmetric excitation at Mach $M = 1.2$ lies considerably closer to the boundary than the $p-k$ method indicates.

C. Computational Analysis

The μ analysis method of computing flutter margins presents significant analytical advantages due to the robustness of the resulting flutter margin, but it also has several computational advantages over the $p-k$ method. The μ algorithm requires a single linear aeroelastic plant model at a given Mach number to compute critical and subcritical flutter margins. An entire set of flutter margins may be easily generated using a standard engineering workstation in a few minutes using widely available software packages.[6]

The $p-k$ method is an iterative procedure that requires finding a matched-point solution.[19] The aircraft is analyzed at a particular Mach number and air density. The airspeed for these conditions resulting in a flutter instability is computed. This airspeed, however, often does not correspond to the unique airspeed determined by that Mach number and air density for a standard atmosphere. Various air
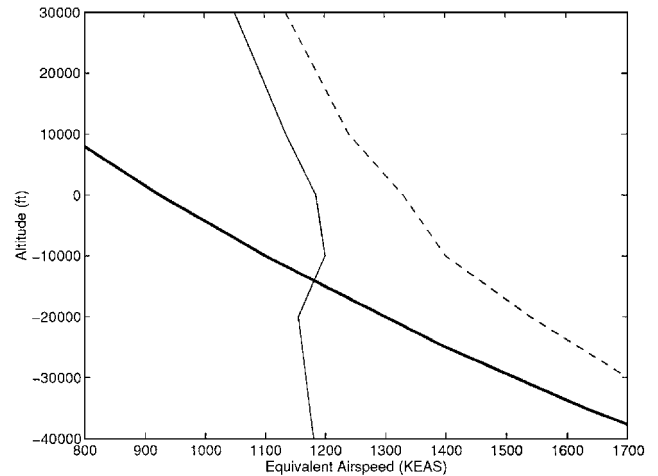

Fig. 6 Antisymmetric $p-k$ flutter solutions for Mach 1.4: ━━━, standard atmosphere; ────, wing second torsion mode; and - - -, trailing-edge flap rotation mode.

densities are used to compute flutter solutions, and the corresponding air speeds are plotted. An example of an airspeed plot from $p-k$ flutter analysis is given in Fig. 6.

The vertical lines in Fig. 6 represent two antisymmetric modes that may flutter at Mach $M = 1.4$. The $p-k$ method computes a flutter solution at the airspeed indicated where the modal line crosses the standard atmosphere curve. This flutter solution is difficult to compute from only a few air density computations. Typically several air densities are used to compute airspeed flutter solutions, and a line is extrapolated between the points to determine the matched-point solution at the standard atmosphere crossing point. The nonlinear behavior shown for the second torsion mode near the standard atmosphere crossing point indicates an accurate flutter boundary would be extremely hard to predict unless many solutions are computed near the true matched-point solution.

The $p-k$ method also may have difficulty predicting the subcritical flutter margins. The second mode in Fig. 6 may or may not intersect the standard atmosphere curve. More computational analysis is required to determine the behavior of this mode at higher airspeeds. The μ-analysis method accurately detects both the critical and subcritical flutter margins without requiring expensive iterations.

VIII. Conclusion

A μ-analysis method of computing flutter margins is introduced. This method analyzes robust stability of a linear aeroelastic model with uncertainty operators. Flight data can be used to formulate the uncertainty operators to accurately account for errors in the model and the range of aircraft dynamics observed due to time-varying aircraft parameters, nonlinearities, and flight anomalies such as test nonrepeatibility. The μ-based approach computes flutter margins that are robust, or worst case, with respect to the modeling uncertainty.

Nominal and robust flutter margins are computed for the F/A-18 SRA aircraft using μ and $p-k$ methods. The similarity of the nominal flutter margins demonstrates the μ method is a valid tool for computing flutter instability points and is computationally advantageous. Robust flutter margins are generated with respect to an uncertainty set generated by analysis of extensive flight data. These margins are accepted with a great deal more confidence than previous estimates because they directly account for modeling uncertainty in the analysis process. The robust flutter margins indicate the desired F/A-18 SRA flight envelope should be safe from aeroelastic flutter instabilities; however, the flutter margins may lie noticeably closer to the flight envelope than previously estimated.

This method replaces damping as a measure of tendency to instability from available flight data. Because stability norms generally behave smoothly at instability boundaries, this method is recommended for preflight predictions and postflight analysis with a minimum amount of flight time.

References

[1]Bisplinghoff, R., Holt, A., and Halfman, R., *Aeroelasticity*, Addison–Wesley, Reading, MA, 1955, pp. 527–531.

[2]Cooper, J., and Noll, T., "Technical Evaluation Report on the 1995 Specialists Meeting on Advanced Aeroservoelastic Testing and Data Analysis," *Proceedings of the 80th AGARD Structures and Materials Panel*, AGARD-CP-566, Rotterdam, The Netherlands, 1995, pp. T1–T10.

[3]Kehoe, M., "A Historical Overview of Flight Flutter Testing," *Proceedings of the 80th AGARD Structures and Materials Panel*, AGARD-CP-566, Rotterdam, The Netherlands, 1995, pp. 1–15.

[4]Hassig, H., "An Approximate True Damping Solution of the Flutter Equation by Determinant Iteration," *Journal of Aircraft*, Vol. 8, No. 11, 1971, pp. 885–889.

[5]Nissim, E., and Gilyard, G., "Method of Experimental Determination of Flutter Speed by Parameter Identification," NASA TP-2923, June 1989.

[6]Balas, G., Doyle, J., Glover, K., Packard, A., and Smith, R., *μ-Analysis and Synthesis Toolbox: Users Guide*, The MathWorks, Natick, MA, 1991.

[7]Fan, M., Tits, A., and Doyle, J., "Robustness in the Presence of Mixed Parametric Uncertainty and Unmodeled Dynamics," *IEEE Transactions on Automatic Control*, Vol. 36, Jan. 1991, pp. 25–38.

[8]Gupta, K., Brenner, M., and Voelker, L., "Development of an Integrated Aeroservoelastic Analysis Program and Correlation with Test Data," NASA TP-3120, May 1991.

[9]Gupta, K., "STARS—An Integrated General Purpose Finite Element Structural, Aeroelastic, and Aeroservoelastic Analysis Computer Program," NASA TM-101709, Jan. 1991.

[10]Giesing, J., Kalman, T., and Rodden, W., "Subsonic Unsteady Aerodynamic for General Lattice Method, Part I—Vol. I—Direct Application of the Nonplanar Doublet Lattice Method," U.S. Air Force Flight Dynamics Lab., AFFDL-TF-71-5, Dayton, OH, Nov. 1971.

[11]Appa, K., "Constant Pressure Panel Method for Supersonic Unsteady Airloads Analysis," *Journal of Aircraft*, Vol. 24, No. 10, 1987, pp. 696–702.

[12]Roger, K., "Airplane Math Modeling Methods for Active Control Design," AGARD CP-228, Aug. 1977.

[13]Kumar, A., and Balas, G., "An Approach to Model Validation in the μ Framework," *Proceedings of the 1994 American Control Conference*, Baltimore, MD, 1994, pp. 3021–3026.

[14]Lind, R., and Brenner, M., "Incorporating Flight Data into a Robust Aeroelastic Model," *Journal of Aircraft* (to be published).

[15]Brenner, M., Lind, R., and Voracek, D., "Overview of Recent Flight Flutter Testing Research at NASA Dryden," AIAA Paper 97-1023, April 1997.

[16]Reed, W., III, "A New Flight Flutter Excitation System," Proceedings, Society of Flight Test Engineers, 19th Annual Symposium, Arlington, TX, Aug. 1988.

[17]Vernon, L., "In-Flight Investigation of a Rotating Cylinder-Based Structural Excitation System for Flutter Testing," NASA TM-4512, June 1993.

[18]Feron, E., and Paduano, J., "Advanced Techniques for Flutter Clearance," NASA Final Rept., Project DFRCU-95-025, Nov. 1995–Oct. 1996.

[19]Voelker, L., "F-18/SRA Flutter Analysis Results," NASA TM (to be published).

[20]Lind, R., and Brenner, M., "Worst-Case Flutter Margins from F/A-18 Aircraft Aeroelastic Data," AIAA Paper 97-1266, April 1997.